Supplementary Information for:

Asymmetrical Calcium Ions Induced Stress and Remodeling in Lipid Bilayer Membranes

Chang Liu[1,2], Qi Zhong[3], Kai Kang[1,2], Rui Ma[*,3], and Chen Song[*,1,2]

[1]*Peking-Tsinghua Center for Life Sciences, Academy for Advanced Interdisciplinary Studies, Peking University, Beijing, China*

[2]*Center for Quantitative Biology, Academy for Advanced Interdisciplinary Studies, Peking University, Beijing, China*

[3]*College of Physical Science and Technology, Xiamen University, Xiamen, China*

[*]E-mail: c.song@pku.edu.cn (CS), ruima@xmu.edu.cn (RM)

1 Results for type (ii) deformation

In the absence of Ca^{2+}, the membrane is spherical with a radius of $R_0 = 0.5$ μm, and the parameters include $\kappa = 20\ k_B T$, $p = 1$ kPa and $\sigma = 0.25$ pN/nm. For the locally impacted case, the impacted area is $a_0 = 0.031$ μm^2 which occupies 1% of the total surface area. As a result of the asymmetric Ca^{2+} induced spontaneous curvature c_0, the spherical shape is deformed into various shapes. In the main text, we assumed that the total surface area of the membrane A is conserved for different deformations, and use the membrane tension σ as a Lagrangian multiplier to impose this condition. The volume V enclosed by the vesicle is allowed to change in response to the induced spontaneous curvature c_0, while the pressure p is fixed. Here we present results by assuming the volume V is conserved and the pressure p is a Lagrangian multiplier to impose this condition. The surface area is allowed to change in response to the varied spontaneous curvature c_0, while the membrane tension σ is fixed. For the local change, the results are almost indistinguishable from the type (i) deformation (Compare Fig. 6 and S8). For the glocal change, the general trends are similar except that the multiplets in general have a higher height in the conserved volume condition than in the conserved surface area condition. (Compare Fig. 7B and S9B).

2 Supplementary Table

Table S1: Coordinated groups within the first shell (3.2 Å) of membrane-bound Ca^{2+}.

Lipid Bilayer	$[Ca^{2+}]$ (mM)	Ca^{2+} Model	Coordination Number		
			POPC $PO4^-$	POPS $PO4^-$	POPS COO^-
POPC	200	Cam	1.19 ± 0.09	-	-
		Cal	1.03 ± 0.05	-	-
	1000	Cam	1.12 ± 0.03	-	-
		Cal	1.00 ± 0.04	-	-
POPC/POPS	200	Cam	0.64 ± 0.03	0.35 ± 0.05	0.28 ± 0.07
		Cal	0.19 ± 0.03	0.10 ± 0.06	1.13 ± 0.14
	1000	Cam	0.57 ± 0.03	0.29 ± 0.04	0.33 ± 0.04
		Cal	0.22 ± 0.01	0.12 ± 0.03	0.91 ± 0.03

3 Supplementary Figures

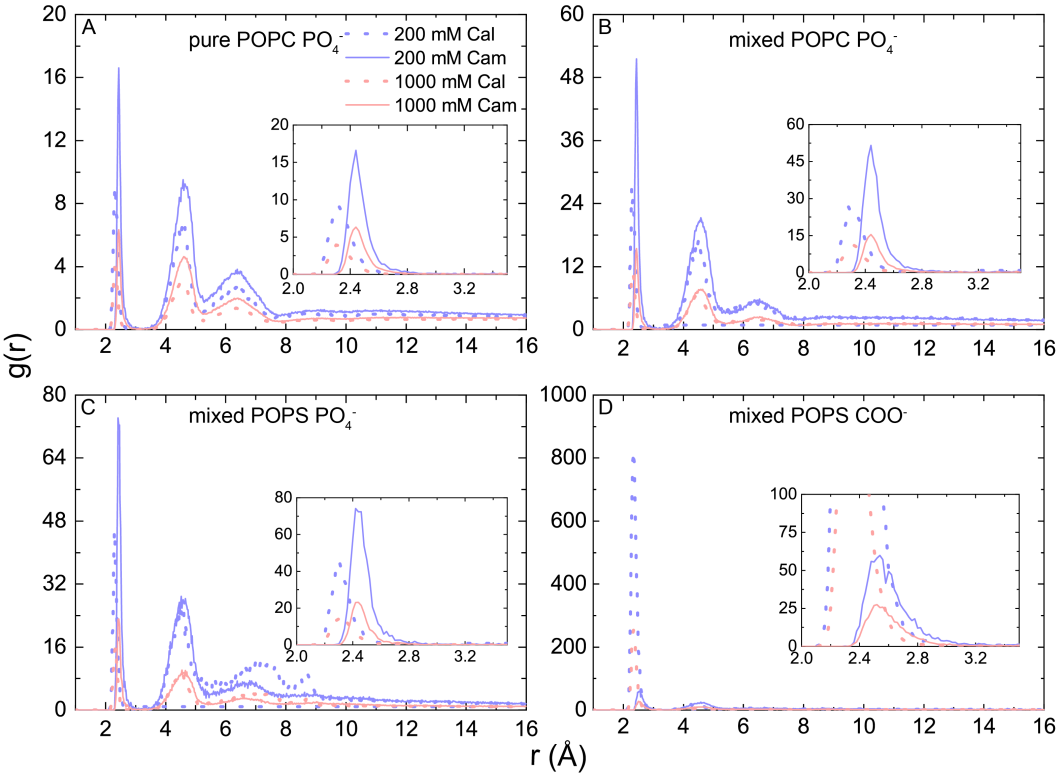

Figure S1: The radial distribution function of Ca^{2+} ions around different lipid oxygen groups. (A) The radial distribution function of two Ca^{2+} models around PC phosphate oxygen atoms in the pure POPC bilayer. (B, C, D) The radial distribution function of two Ca^{2+} models around PC phosphate oxygen atoms (B), PS phosphate oxygen atoms (C), and carboxylate oxygen atoms (D) in the mixed POPC/POPS bilayer. The simulation systems were treated with 200 mM (pink) or 1000 mM Ca^{2+} (blue-violet). The solid lines were obtained using the *Cam* model, while the dashed lines were obtained using the *Cal* model.

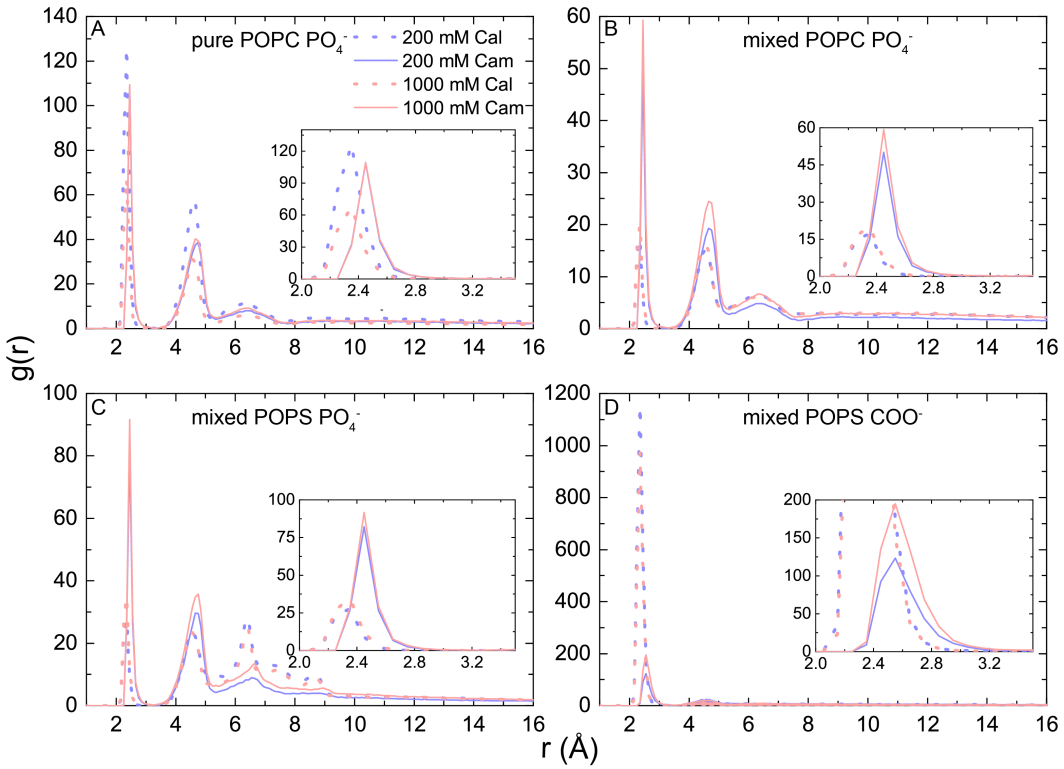

Figure S2: The radial distribution function of different lipid oxygen groups around the membrane-bound Ca^{2+} ions that were within 3.2 Å of lipids. (A) The radial distribution function of PC phosphate oxygen atoms around the membrane-bound Ca^{2+} ions in the pure POPC bilayer. (B, C, D) The radial distribution function of PC phosphate oxygen atoms (B), PS phosphate oxygen atoms (C), and carboxylate oxygen atoms (D) around the membrane-bound Ca^{2+} ions in the mixed POPC/POPS bilayer. The simulation systems were treated with 200 mM (pink) or 1000 mM Ca^{2+} (blue-violet). The solid lines were obtained using the *Cam* model, while the dashed lines were obtained using the *Cal* model.

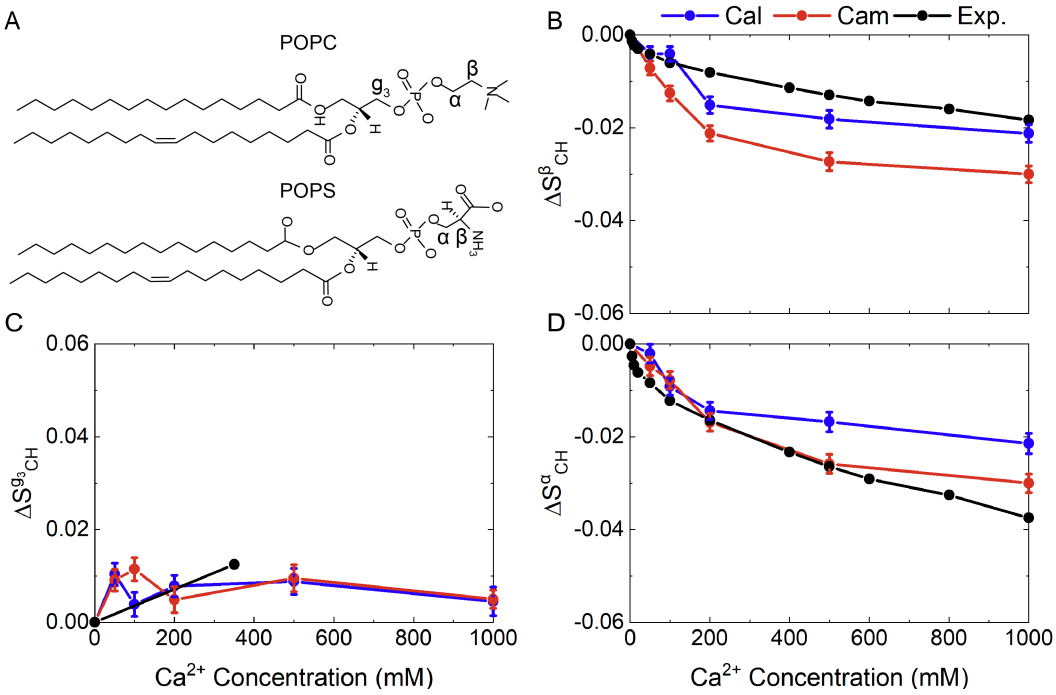

Figure S3: Changes of the headgroup order parameters of pure POPC bilayers with increasing $CaCl_2$ concentrations. (A) Chemical structures of POPC and POPS, and labeling of carbon segments. Changes of the order parameters for the β, α, and g_3 carbon segments in pure POPC bilayer systems were shown in (B), (C), and (D), respectively. The changes of the headgroup order parameters were obtained by subtracting the order parameters of the system without Ca^{2+} from those with Ca^{2+} (ΔS_{CH}). We calculated the time-averaged order parameter for each lipid, and then calculated the mean value as well as the standard error of the mean for all the lipid molecules in the simulation system. The simulation results using the *Cal* and *Cam* models at 313 K, as well as the experimental data, were shown for comparison.

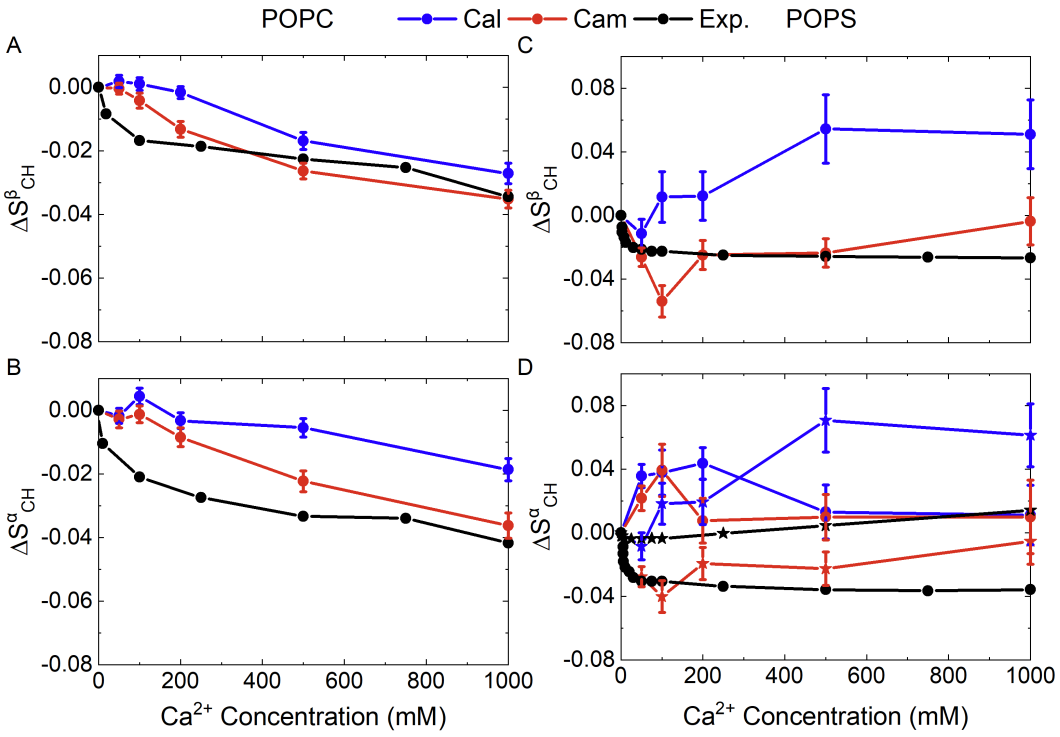

Figure S4: Changes of the headgroup order parameters in a POPC/POPS (5:1) bilayer with increasing $CaCl_2$ concentrations. The changes of β and α carbon segments of POPC were shown in (A) and (B), while those of POPS were shown in (C) and (D). The inequivalence of the two $\alpha - CD2$ deuterons in POPS lipids results in the generation of two distinct α values, denoted as α_1 and α_2 (line and circles for α_1, line and stars for α_2 in panel D). The simulation results using the *Cal* and *Cam* models at 298 K, together with experimental data, were shown for comparison. Please refer to Fig. S3 for the relevant chemical structures and analysis methods.

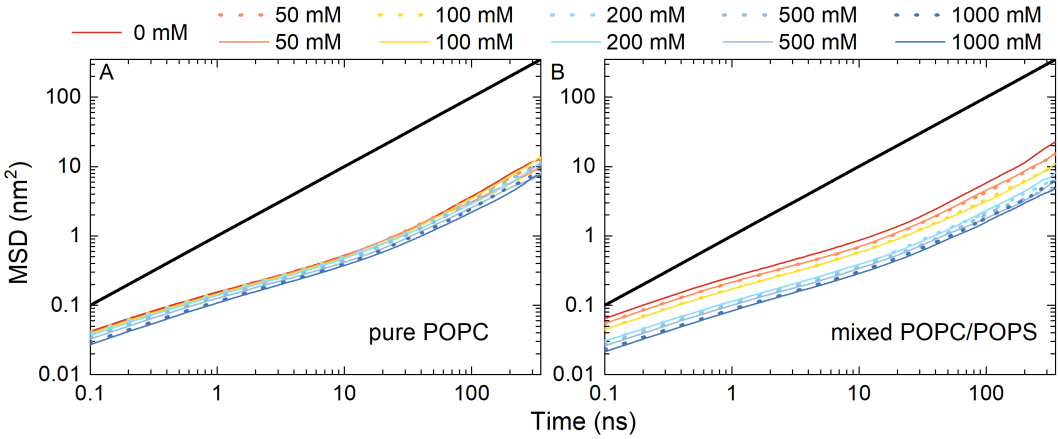

Figure S5: The 2D mean square displacement (MSD) of lipid molecules in the pure POPC bilayer systems (A) and mixed POPC/POPS bilayer systems (B), treated with different Ca^{2+} concentrations. The solid lines were obtained using the *Cam* model, while the dashed lines were obtained using the *Cal* model.

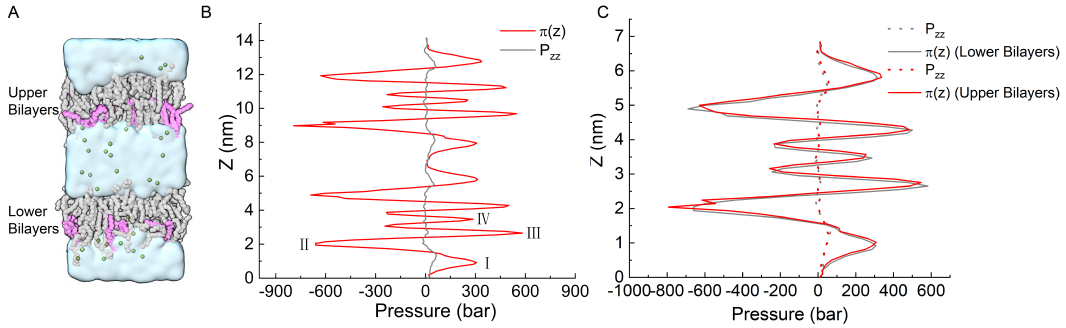

Figure S6: The lateral pressure profile of the double-membrane simulation system without Ca^{2+}. (A) Two asymmetric lipid bilayer membranes. PC lipids were shown in gray, while PS lipids were shown in pink. (B) Lateral pressure profiles calculated from the simulation system with no Ca^{2+}. (C) Aligned lateral pressure profiles of the double-membrane system.

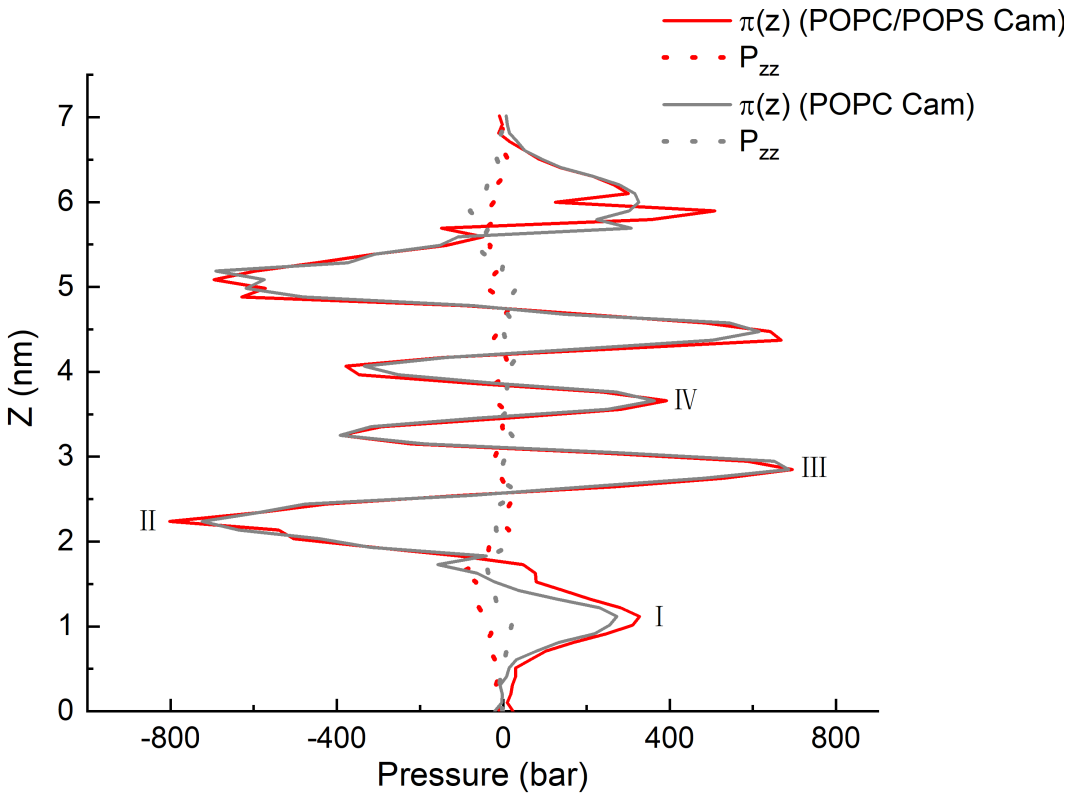

Figure S7: Aligned lateral pressure profiles of the double-membrane system as shown in Fig. 5. The red lines or dots were calculated for the membrane with POPC/POPS facing Ca^{2+} (the upper membrane in Fig. 5A). The grey lines or dots were calculated for the membrane with POPC facing Ca^{2+} (the lower membrane in Fig. 5A).

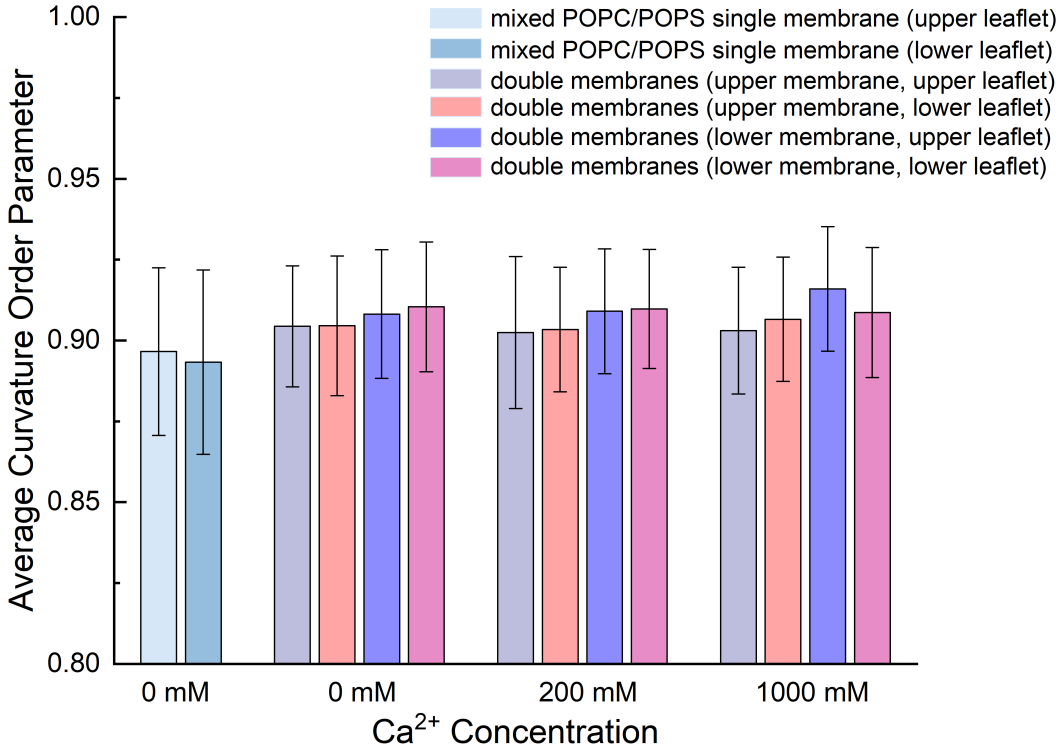

Figure S8: The curvature order parameters of the membranes in different simulation systems. The two histograms on the left show the calculation results for the mixed PC/PS planar membrane. The other histogram groups represent the results of the four leaflets from top to bottom as shown in Figure 5A.

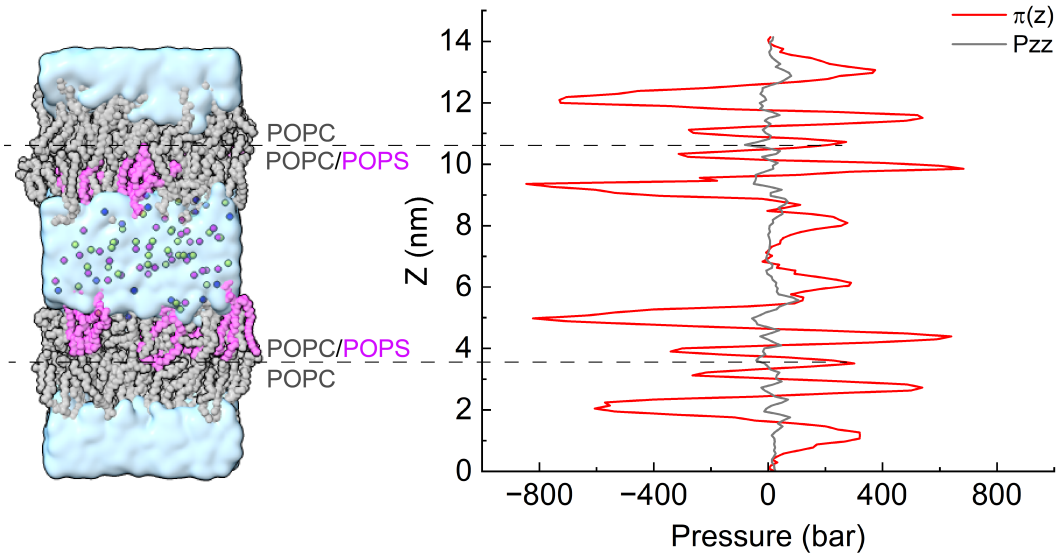

Figure S9: Lateral pressure profiles of the double-membrane system, in which the lower membrane was inverted compared to Fig. 5A, were obtained after treatment with 200 mM Ca^{2+}.

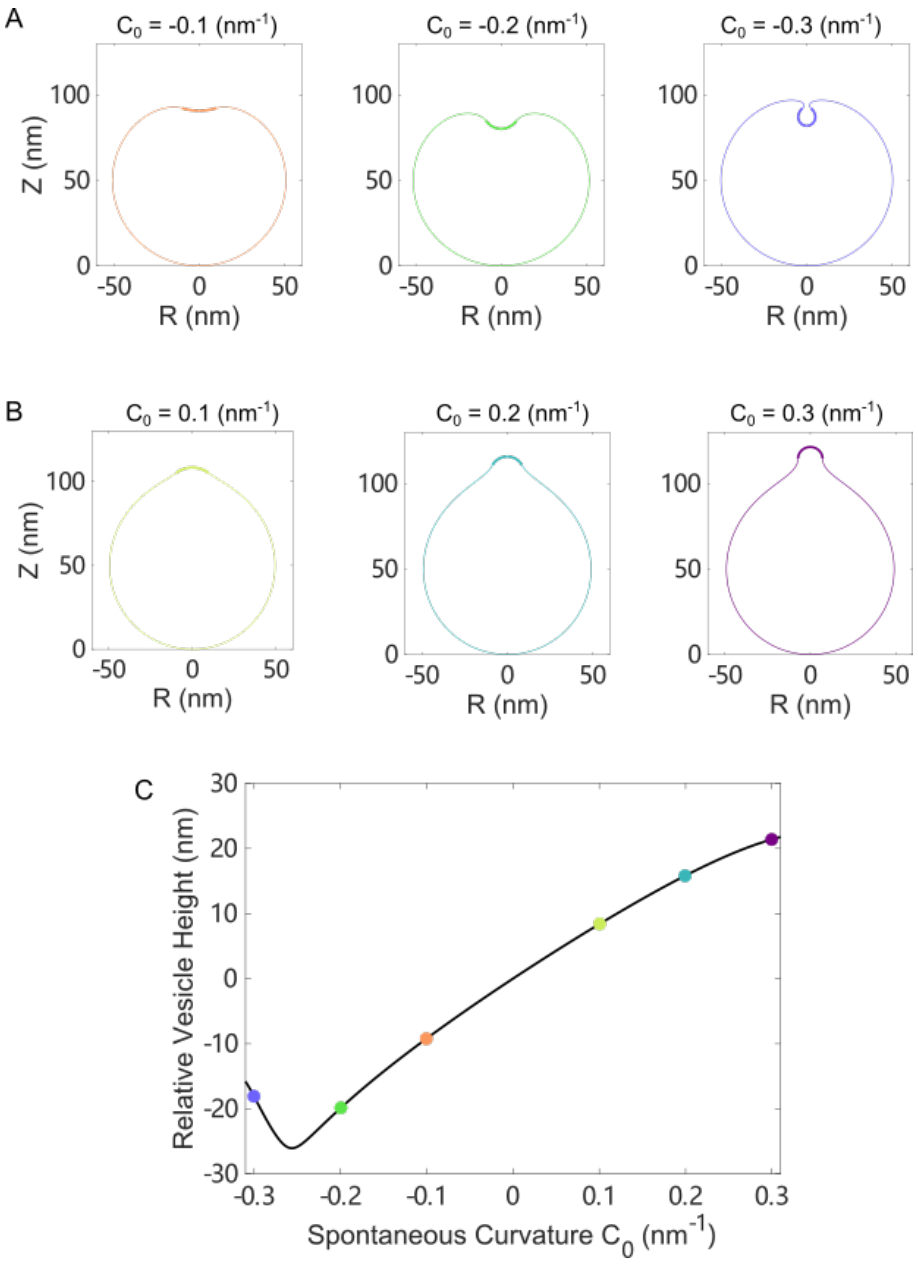

Figure S10: Membrane deformation induced by asymmetric Ca^{2+} concentration between the exterior and interior of a spherical vesicle. The impacted area was localized to a neighborhood of the north pole of the vesicle. The volume enclosed by the vesicle was conserved and the membrane tension was fixed when varying the spontaneous curvature. (A) Membrane shapes in the minimal energy state for negative spontaneous curvature c_0. (B) Membrane shapes in the minimal energy state for positive spontaneous curvature c_0. (C) The relative height of the deformed vesicle as a function of c_0. The dots in (C)correspond to shapes presented in (A) and (B) of the same color.

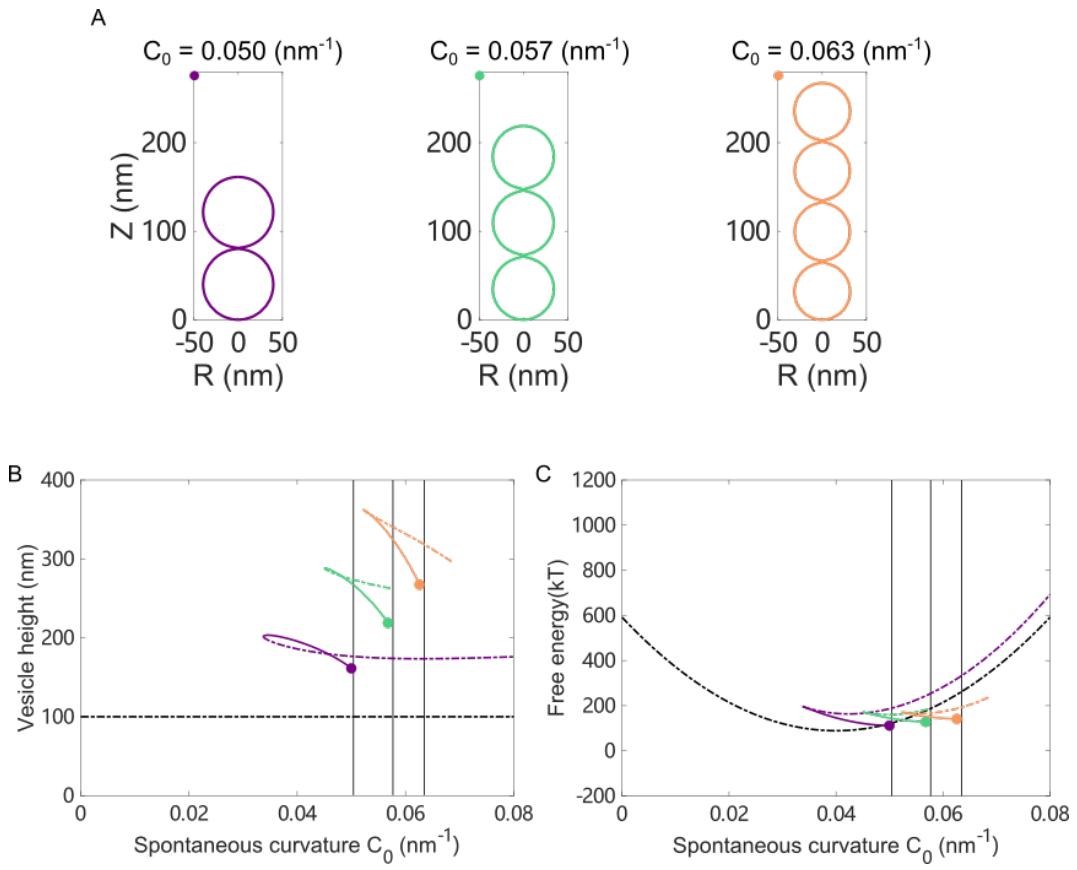

Figure S11: Membrane deformation induced by asymmetric Ca^{2+} concentration between the exterior and interior of a spherical vesicle. The impacted area covered the entire membrane. The volume enclosed by the vesicle was conserved and the membrane tension was fixed when varying the spontaneous curvature. (A) Membrane shapes in the minimum energy state with increasing positive spontaneous curvature c_0. (B) The height of a deformed vesicle as a function of the spontaneous curvature c_0. Branches of singlet (black), duplet (blue), triplet (red) and tetraplet (green) were shown respectively. (C) The free energy of the vesicles in different branches. For each branch, the lower energy part was shown in solid lines and the higher energy part was shown in dash-dotted lines. The vertical lines in (B) and (C) indicate the critical spontaneous curvature $c_0^{\text{crit}} = 2\sqrt{n}/R_0$, where $n = 2, 3, 4$, respectively. The dots in (B) and (C) correspond to shapes presented in (A) of the same color.

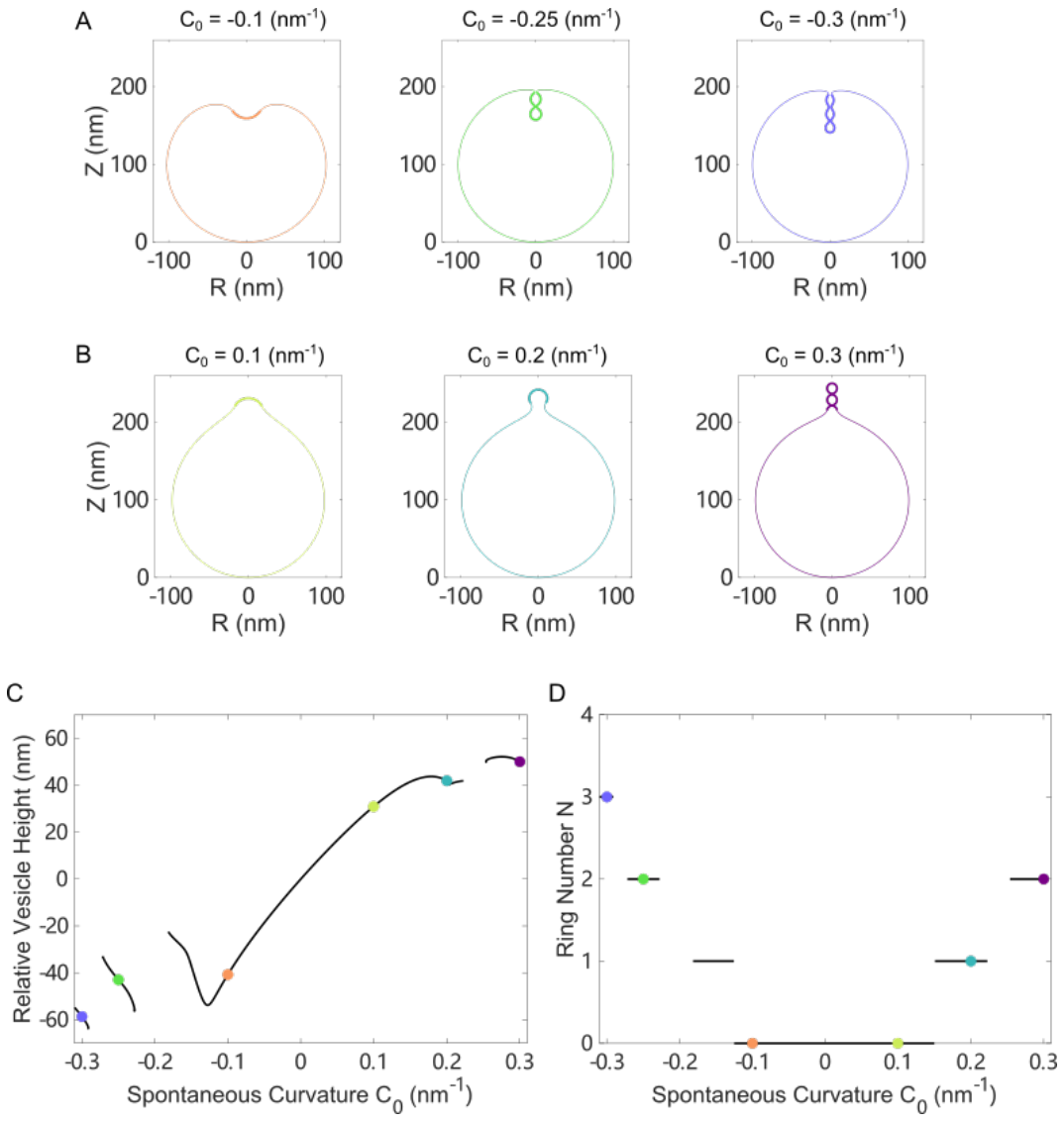

Figure S12: Membrane deformation induced by asymmetric Ca^{2+} concentration between the exterior and interior of a spherical vesicle. The impacted area was localized to a neighborhood of the north pole of the vesicle. The volume enclosed by the vesicle was conserved and the membrane tension was fixed when varying the spontaneous curvature. The diameter of the vesicle was $200\,\mathrm{nm}$. (A) Membrane shapes in the minimal energy state for negative spontaneous curvature c_0. (B) Membrane shapes in the minimal energy state for positive spontaneous curvature c_0. (C) The relative height of the deformed vesicle as a function of c_0. (D) The number of pearls formed on the impacted area as a function of c_0. The dots in (C) and (D) correspond to shapes presented in (A) and (B) of the same color.